Available online at www.sciencedirect.com

SCIENCE DIRECT®

Earth and Planetary Science Letters 241 (2006) 493–504

EPSL

www.elsevier.com/locate/epsl

Interpretation of the $^{231}Pa/^{230}Th$ paleocirculation proxy: New water-column measurements from the southwest Indian Ocean

Alex L. Thomas [a,*], Gideon M. Henderson [a], Laura F. Robinson [a,b]

[a] *Department of Earth Sciences, Oxford University, Parks Road, Oxford, OX1 3PR, UK*
[b] *California Institute of Technology, MS 100-23, 1200 East California Boulevard, Pasadena, CA 91125, USA*

Received 18 March 2005; received in revised form 16 September 2005; accepted 23 November 2005
Available online 3 January 2006
Editor: E. Boyle

Abstract

Measurements of ^{231}Pa, ^{230}Th and ^{232}Th concentrations have been made on five water-column profiles along the western margin of the Madagascar and Mascarene Basins in the southern Indian Ocean. These measurements help to fill a significant gap in the global coverage of water-column ^{232}Th, ^{230}Th and ^{231}Pa data. ^{232}Th concentrations vary, but generally increase with depth, suggesting higher particle loading in deeper waters, and the presence of a significant dissolved fraction of ^{232}Th. ^{230}Th concentrations increase with depth, and profiles are similar to the average of existing data from other regions. ^{231}Pa concentrations, on the other hand, show significant depth structure, apparently reflecting the various water masses sampled at this location. The modified remnants of North Atlantic Deep Water are found at a depth of ≈ 2000 m and exhibit elevated ^{231}Pa concentrations exported from the South Atlantic. Antarctic Intermediate and Bottom Waters have lower ^{231}Pa, probably due to scavenging onto opal particles during transit from the Southern Ocean. The differences between water masses raises a question: which water mass is important in controlling the $^{231}Pa/^{230}Th$ ratio in underlying sediments? A simple one-dimensional model is used to demonstrate that the ^{230}Th and ^{231}Pa exported to sea-floor sediments last equilibrates with waters close to the seafloor (within ≈ 1000 m), rather than averaging the whole water column. These findings suggest that $^{231}Pa_{xs}/^{230}Th_{xs}$ in sediments provides information primarily about deep-water masses. In this region, sedimentary records will therefore provide information about the past flow of Antarctic Bottom Water into the Indian Ocean. Interpretation of data from other regions, such as the North Atlantic where this proxy has most successfully been applied, requires careful consideration of regional oceanography and knowledge of the composition of the water masses being investigated.

Keywords: thorium; protactinium; seawater; Indian Ocean; ocean circulation

1. Introduction

The global thermohaline circulation plays a crucial role in the climate system through its transport of heat and carbon [1]. Tracers used to investigate the past behaviour of the thermohaline circulation have often been those that label a particular water mass, such as $\delta^{13}C$ [2], Cd/Ca [3], or Nd isotopes [4]. Tracers that provide information about the rate of flow of these water masses have also been applied, including ^{14}C [5,6], sortable silt [7,8] and $^{231}Pa/^{230}Th$ [9–13]. The use of $^{231}Pa/^{230}Th$ for this purpose has only previously been assessed in the Atlantic basin. Here, we investigate the controls on $^{231}Pa/^{230}Th$ recorded in deep-sea sediments in a region of more complex oceanography

---

* Corresponding author.
E-mail address: alext@earth.ox.ac.uk (A.L. Thomas).

0012-821X/$ - see front matter © 2005 Elsevier B.V. All rights reserved.
doi:10.1016/j.epsl.2005.11.031

and assess the feasibility of using $^{231}Pa/^{230}Th$ to learn about past deep-water inflow to the Indian Ocean.

The $^{231}Pa/^{230}Th$ proxy relies on decay of uranium dissolved in the oceans. The high solubility of uranyl carbonate makes U a conservative element with a residence time of ≈ 400 ka. The concentration and isotope composition of U in the oceans is therefore constant, both spatially [14,15] and temporally [16]. The production of ^{230}Th and ^{231}Pa, from decay of ^{234}U and ^{235}U, respectively, is thus constant at every point in the oceans (at $2.62 \pm 0.05 \times 10^{-2}$ and $2.45 \pm 0.05 \times 10^{-3}$ dpm m^{-3} a^{-1}, respectively). The production activity ratio of $^{231}Pa/^{230}Th$ is also constant at a value of 0.093. Once produced, both Th and Pa are scavenged to the seafloor through sorption onto particles which subsequently settle. This scavenging of Th and Pa is thought to be reversible [17], which explains the increase of concentration typically seen with water depth for both nuclides. ^{230}Th and ^{231}Pa are removed from the upper water column, and a portion released by reversible exchange at greater depth. A newly ventilated water mass therefore typically has low concentrations of both nuclides, similar to surface waters, and the concentrations increase with time spent at depth in the oceans. Eventually, deep waters reach equilibrium, with the rate of addition of Th or Pa from above balanced by the removal to the seafloor.

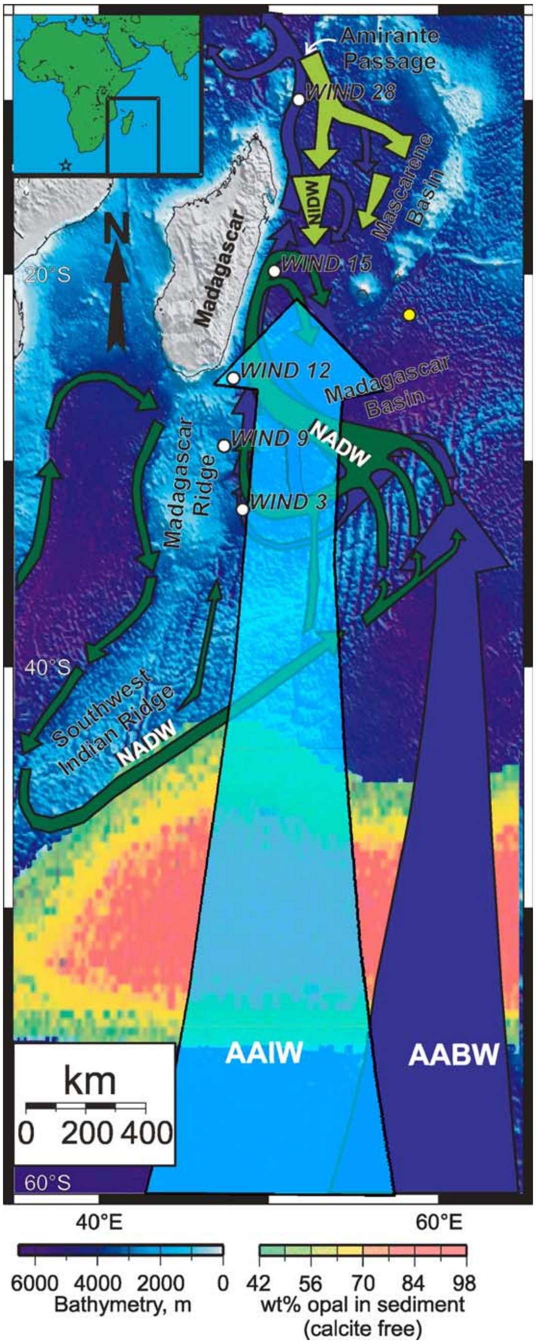

Fig. 1. Location map. A map showing the localities of the water-column profiles measured in this study (white circles). The yellow circle indicates the position of an existing sediment analysis [45]. Also shown schematically are the principal water masses of the region and their flow through the Madagascar and Mascarene Basins. The position of the opal belt, illustrated by the weight percent opal in sediments, taken from a Si cycle model [46], is also shown. Note that the transit of AABW (dark blue) and AAIW (light blue) from the Southern Ocean takes it through the opal belt, while water sources from the Atlantic (referred to here as "NADW," although its salinity is somewhat modified from true NADW values) are confined as a boundary current and avoid high opal productivity on its way to the Madagascar Basin. North Indian Deep water, NIDW, is also shown (light green) and impacts the most northerly of the studied sites. Inset locating the study area shows, as a star, the position of the closest existing water column profile [24] used for comparison in the text.

^{230}Th is removed more rapidly than ^{231}Pa and thus has a shorter oceanic residence time of about 20 yr, compared to 130 yr for ^{231}Pa [18]. As a deep-water mass ages, the concentration of ^{230}Th rapidly reaches a steady-state value while ^{231}Pa takes longer and is therefore expected to be at low concentration for greater distances as deep waters move away from their site of formation. In these areas, the $^{231}Pa/^{230}Th$ of particles settling to the sediment is expected to be below the production ratio of 0.093, while in regions far from the water source, the ^{231}Pa will have increased to steady state and the $^{231}Pa/^{230}Th$ exported to the sediment is 0.093. The effective "age" of the water since ventilation is therefore reflected by the $^{231}Pa/^{230}Th$ removed to sediment, providing a tool to assess the rate of flow of waters in past times. Maps of sediment $^{231}Pa/^{230}Th$ have been used in this way to indicate little change in overall meridional overturning in the Atlantic between the Last Glacial Maximum and the Holocene [9,13].

More recently, time series studies by McManus et al. [10,11] have been used to investigate changes in overturning circulation rate in the North Atlantic accompanying millennial climate changes.

The ^{231}Pa/^{230}Th preserved in sediments is also affected by other factors. The degree to which Pa and Th are fractionated onto particles has been shown to vary for different particle types [19–22]. Although controversy still remains about this particle type dependence [23], it is clear that changes in the particle type do have a role in controlling sedimentary ^{231}Pa/^{230}Th. Scavenging intensity is also a factor controlling the ^{231}Pa/^{230}Th preserved, because in regions of high particle flux, ^{231}Pa will be more efficiently scavenged, hence increasing sedimentary ^{231}Pa/^{230}Th. Boundary scavenging–the process of diffusion of nuclides to ocean margins to be preferentially scavenged there–can also play a role in setting sedimentary ^{231}Pa/^{230}Th.

These other controls on ^{231}Pa/^{230}Th mean that, where deep waters were not recently at the surface, the influence of ocean circulation on sedimentary ^{231}Pa/^{230}Th may be less clear. The effects of complex hydrography and variable water-mass history may also lead to more complex behaviour of ^{231}Pa and ^{230}Th in the water column, even in regions where circulation is fast so that advection of the nuclides dominates over diffusion. The use of ^{231}Pa/^{230}Th to assess rates of past ocean circulation in regions outside the Atlantic therefore requires study of the controls on ^{231}Pa and ^{230}Th in waters and sediments of such these regions. Here we perform such a study in the southwestern Indian Ocean. This region features several water masses, including those originating in the Southern Ocean where ^{230}Th and ^{231}Pa concentrations are typically high [24]. In addition to assessing the controls on these nuclides, this study also provides the first water-column measurements for the southern Indian Ocean and therefore helps to fill a large gap in the growing global coverage of water column ^{231}Pa and ^{230}Th measurements.

2. Regional setting and samples

The movement of deep and bottom water in the SW Indian Ocean features three main water masses moving broadly northward: Antarctic Bottom Water (AABW); a water mass derived from North Atlantic Deep Water, referred to herein as “NADW;” and Antarctic intermediate water (AAIW) (Fig. 1).

AABW enters from the southeast through fracture zones in the Southwest Indian Ridge [25], flowing through the Madagascar and Mascarene Basins and exiting northward through the Amirante Passage. Above this, water derived from NADW flows around the continental margin of southern Africa with characteristics close to that of NADW (salinity 34.80 and potential temperature 2.0–2.5 °C). This “NADW” continues around the Madagascar ridge and then northwards as a geostophically constrained boundary current [26] (Fig. 1), the salinity decreasing through mixing to 34.78 by the time it has reached 25 °S. The flow of NADW and AAIW, however, is impeded by southward movement [27] of two other water masses, North Indian Deep Water and, to a lesser extent, Red Sea Water [28]. The influence of both AAIW and NADW therefore decreases northward, as shown in the temperature and salinity profiles measured for this study (Fig. 2). Overlying these deeper water masses is Indian Central Water (ICW) formed in the subtropical gyres of the Indian Ocean. An overview of the basins' oceanography can be found in McCave et al. [29].

To investigate the behaviour of ^{231}Pa and ^{230}Th in this region of complex oceanography, five water-column profiles (Fig. 1) were sampled along the western margins of the Mascarene and Madagascar Basins during *Charles Darwin* Cruise 129 (McCave 2002, unpublished cruise report). Five to seven 10 l unfiltered water samples were collected per profile making a total of 31 samples. Samples were collected with a rosette of twelve 10 l Niskins fired on the up-cast and stored in acid-rinsed cubitainers. In addition, two samples from

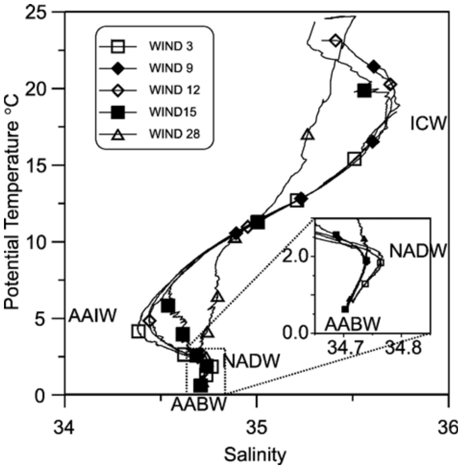

Fig. 2. Hydrography. A plot of potential temperature (°C) against salinity (‰) for CTD casts at stations shown in Fig. 1 (listed in the key from south to north). The approximate position of water masses are shown: ICW, Indian Central Water; AAIW, Antarctic Intermediate Water; “NADW,” modified North Atlantic Deep Water; and AABW, Antarctic Bottom Water. Depths corresponding to these water masses are also indicated on Fig. 4. The inset shows an expansion of the lower section of the profiles. Symbols show positions of samples analysed in this study.

one profile were filtered using a 2 μm inline filter. Filtration was performed in the "wet-lab," aboard the *Charles Darwin* into a glass bottle, before being transferred to the cubitainer. Most of these profiles are sampling northward-flowing water masses from the seafloor to depths of about 1000 m, whereas the most northerly profile (WIND 28) samples a mixture of northward-flowing bottom water and southward-flowing intermediate water.

3. Analytical techniques

Ten litre water samples were weighed and acidified to pH 1 with 7.5N HNO_3. They were then spiked with a mixed ^{229}Th (~500 fg) and ^{236}U (~60 ng) spike (Oxford Water Spike [30]) and a ^{233}Pa spike (~70 fg, $t_{1/2}$ 26.975 days [31]), milked from ^{237}Np by Marcel Regelous at Bristol [32]. Calibration of the ^{233}Pa spike was performed at Oxford by the addition of ^{236}U spike and measurement of $^{236}U/^{233}U$ after all the ^{233}Pa had decayed to ^{233}U. The precision achieved was 1.2% based on two aliquots, and the resulting concentration is consistent with a calibration of the same spike against a secular equilibrium standard performed at Bristol [32]. 10 mg of Fe (previously cleaned by solvent extraction with isopropyl ether) was also added to each water sample before shaking overnight. NH_4 was then added until the pH rose to ~8 to co-precipitate the actinides with insoluble Fe-oxyhydroxides. The neutralised sample was allowed to stand for up to 2 days to allow this Fe precipitate to settle. The majority of the water was siphoned off and the precipitate centrifuged and washed with water. The precipitate was then dissolved in 7.5N HNO_3, dried down and redissolved in 0.5 ml of 7.5N HNO_3 ready for anion exchange chromatography.

Th, Pa and U are separated using Dowex Bio-Rad AG1-X8 100–200 mesh anion exchange resin, held in a 0.5-ml Teflon™ column, following a procedure adapted from Robinson et al. [30]. All acids were quartz distilled, with the exception of HF which was distilled in a Teflon™ still. Water was 18.2 MΩ Milli-Q, and NH_4 is isothermally distilled in a Teflon™ beaker. Columns were washed with 2 ml 7.5N HNO_3, 2 ml 1N HNO_3, 2 ml 6N HCl, 4 ml 1N HNO_3 and preconditioned with 2 ml 7.5N HNO_3. Each sample, dissolved in 0.5 ml 7.5N HNO_3, was loaded and washed in to the column with a further 1.5 ml of 7.5N HNO_3. This washes off Fe and some U. The column was then converted to Cl^- with drops of 6N HCl to 300 μl. Pa and Th were eluted with 2 ml 6N HCl + 0.05N HF. The remaining U is eluted with 2 ml of H_2O. The Pa–Th split was dried, redissolved in 0.5 ml 7.5N HNO_3 and the column repeated to further remove U and to separate Th from Pa by elution with 6N HCl (Th) followed by 6N HCl + 0.05N HF (Pa). Th and Pa splits were dried and dissolved in 10 μl of 7.5N HNO_3, and then diluted to 2% HNO_3 immediately prior to analysis. Care was taken while drying each sample to not fully desiccate the sample which could lead to the formation of insoluble Th and Pa fluorides. Total yields, assessed by the comparative voltage of the spike isotopes against a standard of known concentration, were poor at only ~20% (Pa) and ~40% (Th). Loss is thought to occur during co-precipitation rather than anion exchange, as yields for blanks, which were precipitated from a smaller volume

	STEP	F(+7)	F(+5)	F(+3)	F(+2)	F(+1)	AXIAL	F(-1)	F(-2)	IC(-3)	F(-4)	IC(-5)	F(-6)	IC(-7)	F(-8)
Bracketing standard	1						238			235					
	2								238			235			
	3					238			235			╳			
Th	4					235			232	╳	230	229			
	5			238			235			╳		230	229		
Pa	6				238		236	235		233	232	231		229	

Fig. 3. Schematic showing all collectors of the Nu instruments MC-ICP-MS with the most significant isotopes collected during measurement of Pa and Th. Ion counter gain and mass discrimination are assessed before each sample by measurement of the CRM-145 U standard using Steps 1–3. Steps 1 and 2 assess the gain of the two ion counters to be used, and Step 3 the mass discrimination. These standard measurements were followed by measurement of either Th (Steps 4 and 5) or Pa (Step 6). Th was analysed using a two-step procedure with ^{229}Th and ^{230}Th measured sequentially in an ion counter equipped with an energy filter to improve abundance sensitivity (IC-5) while beam instability was corrected by measurement of ^{235}U in Faraday collectors during both steps. Pa was measured statically with ^{233}Pa and ^{231}Pa in two ion counters. ^{236}U was also monitored to check for clean separation of U during chemistry, and ^{232}Th to assess the importance of ^{232}ThH+ and peak tails on adjacent masses. The contributions to masses 233 and 231 from any ^{232}ThH or peak tails from ^{232}Th are assessed by bracketing Pa measurements with a measurement of a ^{232}Th standard. Separation of Pa from Th reduced the magnitude of the correction for interferences from ^{232}ThH and abundance sensitivity to within the uncertainty of the uncorrected measurement.

Table 1
^{231}Pa and ^{230}Th concentrations and isotope ratios

Sample	Latitude (°S)	Longitude (°E)	Water depth (m)	Depth (m)	^{230}Th (dpm /1000 l)	2 S.E.	^{231}Pa (dpm /1000 l)	2 S.E.	^{232}Th (dpm /1000 l)	2 S.E.	(^{231}Pa/^{230}Th)	2 S.E.	(^{230}Th/^{232}Th)	2 S.E.
WIND 3–11+12	32.39.05	48.28.16	3728	150	0.04	0.15	0.040	0.006	0.006096	0.000003	1	4	6	24
WIND 3–10				450	– 0.59[a]	– 0.40	0.039	0.005	0.007003	0.000005	– 0.07[a]	– 0.04	– 86[a]	– 57
WIND 3–9				1200	8.7[a]	1.9	0.10	0.01	0.00084	0.00001	0.01[a]	0.003	10000[a]	2500
WIND 3–8				1780	0.43	0.10	0.24	0.03	0.008533	0.000005	0.56	0.15	50	12
WIND 3–7				2750	0.71	0.10	0.32	0.04	0.009591	0.000005	0.45	0.08	74	10
WIND 3–5f				3250	1.13	0.19	0.26	0.03	0.06673	0.00004	0.23	0.05	17	3
WIND 3–4				3753	1.13	0.12			0.01991	0.00001			57	6
WIND 3–2f				3753	1.03	0.11			0.07988	0.00005			13	1
WIND 9–10	29.24.27	47.22.25	3334	75	0.136	0.004	0.08	0.01	0.00417	0.0006	0.62	0.11	33	5
WIND 9–8				250	0.156	0.009	0.06	0.01	0.00471	0.0008	0.38	0.11	33	8
WIND 9–7				500	0.249	0.006	0.07	0.01	0.00760	0.0009	0.29	0.06	33	6
WIND 9–6				750	0.349	0.006	0.11	0.02	0.012	0.002	0.32	0.07	29	6
WIND 9–4				2000	0.460	0.005	0.32	0.04	0.009	0.001	0.70	0.08	52	7
WIND 12–11+12	25.50.53	47.55.17	4186	38	0.120	0.005	0.03	0.02	0.008	0.002	0.26	0.15	14	4
WIND 12–9				170	0.108	0.003	0.04	0.01	0.00319	0.0007	0.38	0.11	34	8
WIND 12–7				650	0.264	0.006	0.10	0.02	0.008	0.001	0.38	0.08	35	6
WIND 12–6				1100	0.57	0.02	0.17	0.06	0.017	0.005	0.31	0.12	33	12
WIND 12–5				2700	0.79	0.02	0.34	0.09	0.016	0.004	0.43	0.14	50	16
WIND 15–12	20.00.01	50.19.93	4629	170	0.07	0.03	0.038	0.005	0.003665	0.000002	0.54	0.22	19	7
WIND 15–11				500	0.16	0.05	0.03	0.01	0.007585	0.000004	0.21	0.09	21	7
WIND 15–10				900	0.31	0.04	0.12	0.01	0.005072	0.000003	0.38	0.06	62	7
WIND 15–9				1250	0.35	0.05	0.19	0.02	0.010093	0.000005	0.54	0.10	35	5
WIND 15–8				1750	0.77	0.11	0.29	0.03	0.011439	0.000006	0.37	0.07	68	10
WIND 15–7				2500	0.76	0.09	0.26	0.03	0.012211	0.000007	0.34	0.06	62	8
WIND 15–4				4400	0.93	0.10	0.19	0.02	0.014323	0.000007	0.20	0.03	65	7
WIND 28–9	10.09.85	51.45.74	4137	100	0.167	0.009	0.07	0.009	0.007713	0.000004	0.40	0.06	22	1
WIND 28–8				300	0.32	0.02	0.09	0.01	0.013193	0.000007	0.28	0.04	24	1
WIND 28–7				900	0.44	0.02	0.14	0.02	0.01817	0.00001	0.32	0.04	24	1
WIND 28–6				1400	0.66	0.04	0.19	0.02	0.014902	0.000009	0.28	0.04	45	3
WIND 28–5				2000	0.65	0.06	0.29	0.03	0.04646	0.00002	0.44	0.07	14	1
WIND 28–2				4000	0.82	0.21	0.30	0.03	0.03449	0.00002	0.37	0.11	24	6

Concentrations have been converted to dpm/1000 l assuming 1 fg/kg ^{230}Th = 0.0456 dpm/1000 l and 1 fg/kg ^{231}Pa = 0.105 dpm/1000 l. ^{231}Pa/^{230}Th and ^{230}Th/^{232}Th are expressed as activity ratios. Half-lives used throughout this study are 32.76 ka, 75.690 ka for ^{231}Pa and ^{230}Th, respectively [42,43] and 14.0100 Ga for ^{232}Th [44]. All errors are 2 standard errors and incorporate uncertainty due to raw ratios measured; ion-counter gain; mass discrimination; peak tailing and molecular interference; machine memory; and procedural blank. f denotes a filtered water sample.

[a] These measurements are discounted, as they fall outside the range of sensible values for natural samples.

of liquid, were significantly higher. The yield could be improved in the future by increasing the amount of Fe added to aid co-precipitation. The separation of U from Pa is good with only 0.01% of the initial U in the final Pa fraction (assessed from ^{236}U measurements in the Pa fraction). This is important because a portion of the ^{233}Pa will have decayed to ^{233}U since milking of the spike and this ^{233}U must be quantitatively removed.

Pa and Th were measured on a Nu Instruments MC-ICP-MS using multiple ion counting channels. Mass discrimination and ion-counter gain were measured by preceding each sample analysis with measurement of the CRM-145 U standard (Fig. 3). The use of a U standard for this purpose allows measurement of machine performance directly before Th and Pa analysis without fear of memory effects.

Although the ionisation efficiency of U and Pa are thought to be similar [33], there may be some difference as their first ionisation enthalpies are 5% different (597.6 and 568 kJ mol^{-1}). Pa measurements were therefore always made within a few days of separation to minimise decay of ^{233}Pa to ^{233}U in the Pa cut.

The total uncertainty associated with measurements of ^{231}Pa and ^{230}Th is typically 8–10%. The bulk of this uncertainty (50–75% of the total uncertainty) arises from the raw ratio of $231^+/233^+$ or $230^+/229^+$ measured on the mass spectrometer and is comparable to counting statistics for the total number of ions collected. Somewhat larger uncertainty in this study compared to other measurements of ^{231}Pa and ^{230}Th by ICP-MS [33] is principally due to the poor yield. Corrections for abundance sensitivity, molecular interferences, and mass discrimination are all small and add typically only <0.1% to the total uncertainty. Uncertainty in the ion counter gain can add 0.2%. Machine memory can add 1% if the previous solution is not completely washed out. The calibration of the spike, particularly for ^{233}Pa, is a major contributor to the final uncertainty and along with weighing errors for the sample and spike can add 3% to the final uncertainty. The contribution to uncertainty from the blank is dependent on the total amount of ^{231}Pa or ^{230}Th in the sample, such that for deep samples with high ^{231}Pa and ^{230}Th concentrations, the extra uncertainty due to the blank correction is <0.1%. For surface water samples where ^{231}Pa and ^{230}Th are lower, the blank can add 0.5% of uncertainty to ^{231}Pa and 0.1% to the ^{230}Th measurements. Blanks were determined by performing a complete chemical procedure on ~100 ml of Milli-Q water. A blank was run with each batch of samples, and the mean value taken as the blank for all samples. Although this will include any Th and Pa in the Milli-Q water, it probably represents a slight underestimate of the blank as it discounts any contamination from shipboard processing.

4. Results

All five ^{230}Th profiles show a broadly linear increase in concentration with depth, from ≈ 0.04 dpm/1000 l in surface waters to ≈ 1 dpm/1000 l at 4000 m (Table 1, Fig. 4). Note that, although nuclides were measured as fg/kg, they are converted, for the purposes of discussion, to dpm/1000 l to aid comparison with literature data. These ^{230}Th profiles are similar to the average global profile [18] and to that observed in the Southern Ocean at 44°28.7′°S between 10°27.3′E [24] (Fig. 4).

^{231}Pa profiles show an increase of concentration in the upper half of the water column, from 0.03 dpm/1000 l at the surface to ≈ 0.3 dpm/1000 l at 2500 m, followed by a constant or slightly decreasing concentration in deeper water (Fig. 4). The maximum ^{231}Pa concentration coincides with the presence of NADW, as recognized from

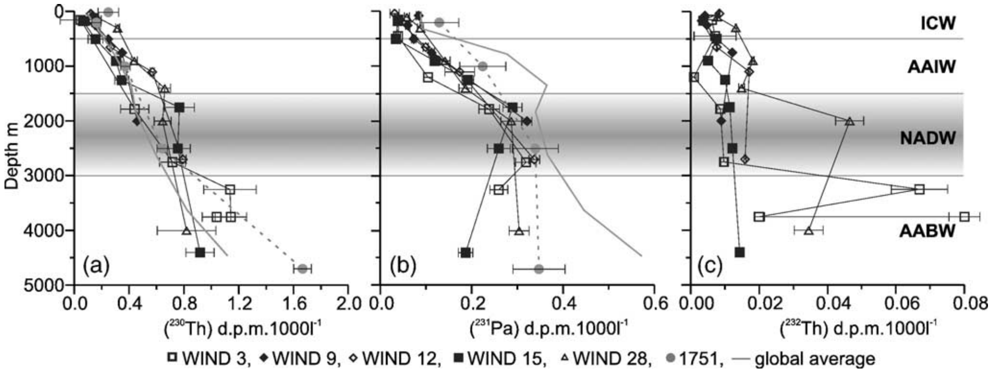

Fig. 4. Water-column results. Concentration profiles through the water column for (a) ^{230}Th; (b) ^{231}Pa; and (c) ^{232}Th. Grey-filled circles with dashed lines are a profile from station 1751 in [24]; the thick grey line is globally averaged data from [18]. Approximate depths of water masses are shown according to T–S data (Fig. 2). All errors are 2 standard errors.

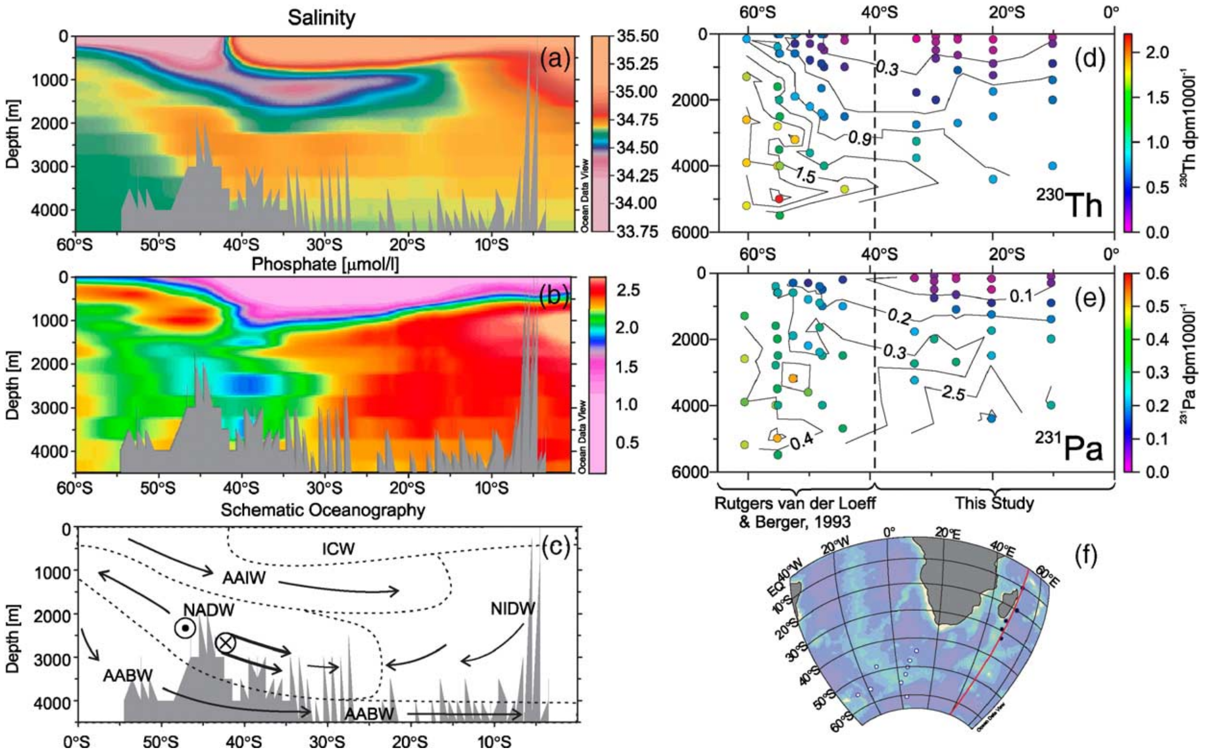

Fig. 5. (a, b) Average salinity and phosphate sections for the western Indian Ocean (i.e., along the red line in panel f), data is taken from the World Ocean Atlas [47,48]. The figure in (c) is a schematic representation of water masses and their movement. Note the movement of low phosphate, "NADW," through the South West Indian Ridge at 45 °S and then back west out of the section following the Madagascar Ridge. (d, e) Sections through the Southern and Indian Oceans showing the concentrations of ^{230}Th and ^{231}Pa. Note that the data in the Southern Ocean [24] is not at the same longitude as that in the Indian Ocean, but that comparison are valid due to similar conditions seen at any latitude in the Southern Ocean. ^{230}Th in the Indian Ocean shows a monotonous increase of concentration with depth. The ^{231}Pa profiles show more structure. Data from the Southern Ocean show no coherent variation, which may reflect larger measurement uncertainty. ^{231}Pa concentrations in the Indian Ocean, however, show elevated values at depths corresponding to NADW.

shipboard T–S data (Fig. 2) and a phosphate minimum in literature data from this area (Fig. 5). Above and below this ^{231}Pa maximum, values are somewhat lower than those in the Southern Ocean, although these waters have recently flowed from this region.

^{232}Th concentrations are typically ≈ 0.01 dpm/1000 l but show significant variation. In particular, three of the deeper samples show much higher concentrations, up to 0.06 dpm/1000 l and, even excepting these samples, there is a slight tendency towards higher concentration at depth.

5. Discussion

5.1. Controls on radionuclide concentrations in Indian Ocean waters

5.1.1. Behaviour of ^{231}Pa and ^{230}Th

Structure observed in the ^{231}Pa profiles measured in this study appears to be controlled by the source and history of the various water masses sampled. Correspondence between high ^{231}Pa and the high-salinity waters of "NADW" indicate that the high ^{231}Pa is a distinct feature of "NADW" in this region. This is seen in Fig. 5, in which new data from this study are compared with data for the Atlantic sector of the Southern Ocean [24]. Although data from the two studies are separated by ≈ 40° of longitude, the zonal similarity of conditions in the Southern Ocean [34], due to strong west–east flow, make such comparison valid. Reasonably continuous values of ^{231}Pa are observed moving from the Southern Ocean northwards. But high ^{231}Pa concentrations are found in the section at ≈ 2500 m water depth and 40 °S (Fig. 5). This is the region where "NADW" is overflowing the southwest Indian Ridge to enter the Madagascar Basin [26]. These high ^{231}Pa values persist northwards, demonstrating that mixing and particle settling do not obscure the differences between water masses on the timescale of transit through the Madagascar Basin.

^{231}Pa concentration in the various water masses measured in this study are likely to be controlled by their source and by scavenging in the Southern Ocean opal belt. "NADW" enters the Madagascar and Mascarene Basins as a geostrophically constrained boundary current around the Southern African Margin and does not enter the Southern Ocean. High ^{231}Pa in these "NADW" samples must, therefore, be attributed to high ^{231}Pa water from the South Atlantic, rather than from the Antarctic Circumpolar Current (ACC). The concentrations of ^{231}Pa in the rest of the water column are lower, and lower than seen in the Southern Ocean from where they are sourced. This is likely to be due to strong removal of Pa from the water column as the water leaves the ACC by scavenging on opal particles which has been shown to strongly favour scavenging of Pa [19,35,36].

The recognition that water masses can have distinct ^{231}Pa concentrations relative to waters above and below, reflecting the differing histories of the water masses, will make interpretation of sedimentary ^{231}Pa/^{230}Th ratios more complex. In contrast to ^{230}Th, which rapidly achieves an equilibrium profile, the greater solubility of ^{231}Pa allows water masses to retain a characteristic ^{231}Pa concentration for considerable distances. It is therefore to be expected that water masses with distinct ^{231}Pa concentrations will be found overlying one another in many areas of the world ocean, just as observed in this area of the southern Indian Ocean. Before sedimentary Pa/Th ratios can be interpreted in such areas, we must understand how each water mass impacts the Pa/Th value recorded in the sediment. This issue is returned to in Section 5.2.

5.1.2. Behaviour of ^{232}Th

Individual profiles typically show a slight increase in ^{232}Th concentration with depth (e.g., WIND 15; Fig. 4) but with a large degree of scatter, especially at depths corresponding to AABW. Unlike ^{230}Th and ^{231}Pa, which are almost entirely derived from decay of U in the water column, ^{232}Th is derived from detrital material derived from aerosols or from the continental margins. The scatter in the ^{232}Th data observed here can be attributed to changing content of such detrital material, because samples in this study were not filtered. The high values and large variability of AABW ^{232}Th are likely to be caused by a dilute expanded nephaloid layer, perhaps influenced by sediment transport from the continental slope of Madagascar. Even excluding the unusually high ^{232}Th values seen in some of these AABW samples, however, a slight increase in concentration with depth persists. If insoluble ^{232}Th-bearing particles settle at a uniform speed throughout the water column, such an increase is not expected. The increase can be explained, however, if some portion of the ^{232}Th is dissolving in seawater and is reversibly scavenged onto sinking particles in a similar manner to ^{230}Th.

5.2. Implications for the use of Pa/Th to reconstruct past ocean circulation in the Indian Ocean

Unlike the modern-day North Atlantic, the water column in the Western Indian Ocean is not dominated by recently ventilated water, but consists of several water masses with different histories and flow rates. To use sedimentary ^{231}Pa/^{230}Th to learn about past water flow in such regions requires an assessment of the depth from which Pa and Th last equilibrate in the water column before reaching the sediment. In other words, we must determine the depth at which the ratio on sedimenting particles is acquired. A common assumption in interpretation of sediment ^{231}Pa/^{230}Th ratios has been that they represent average flow conditions through the entire water column. If this is true, then interpretation of sediment Pa/Th in regions of complex oceanography will always be an ambiguous process. With more than one water mass overlying the sediment core, changes in Pa/Th might represent changes in the flow rate and history of one of these waters, or more than one of them. In this section, we use a simple model to test this assumption and to assess the depth at which particle Pa and Th last exchange with seawater before reaching the sediment.

The majority of ^{230}Th and ^{231}Pa in any water mass is in the dissolved portion (typically ≈ 90%) [18]. During equilibration between recently settled particles and a water mass, therefore, it is the dissolved ^{230}Th and ^{231}Pa which sets the ^{231}Pa/^{230}Th on the particles before they settle further. With sufficient time, the cumulative flux of particles falling through the water mass can change its Pa and Th composition by this equilibration process, but this does not alter the fact that it is the water composition at any particular time and place that sets the composition of downward settling particles. Put another way, the average particle typically settles through the entire water column in about 3 yr which is a short time compared to the deep-water residence times of Th and, particularly, Pa.

To investigate the depth at which Th and Pa are last equilibrated we use a 1D particle scavenging box model which comprises two particle classes: fine particles which do not settle and are effective scavengers because of their high surface area; and coarse particles, formed by the aggregation of the smaller particles, which are responsible for all the downward removal of ^{230}Th and ^{231}Pa from each box (Fig. 6). No scavenging onto these

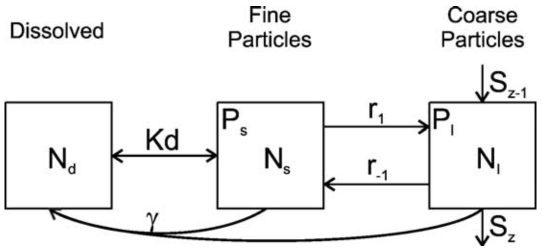

Fig. 6. A schematic representation of the model used to assess the depth from which ^{230}Th and ^{231}Pa are scavenged to the seafloor following [40,49,50]. Dissolved isotopes are scavenged to fine particles, making up the majority of the particle mass, assuming an equilibrium Kd. These fine particles can aggregate (rate=r_1, yr^{-1}) into coarse particles which settle (rate=S, m day^{-1}) while also disaggregating (r_{-1}, yr^{-1}) and dissolving (γ, yr^{-1}). P_l and P_s are the concentration of large and small particles (g m^{-3}).

coarse particles is allowed because of their low surface area-to-mass ratio and because they settle too quickly to allow equilibration as they fall. The effect of eddy diffusion on redistribution of the small particle class is thought to be small [37] and is ignored. The distribution of particles between fine and coarse in the model is governed by aggregation (r_1, yr^{-1}) and disaggregation (r_{-1}, yr^{-1}) constants. The distribution of the nuclides between dissolved and fine particles is calculated from a prescribed distribution coefficient (Kd) and particle concentration. All variables in the model are listed in Table 2, together with values used in the control run. The value of Kd determines the distribution of nuclide between the dissolved phase and the particulate phase, so will affect the rate of removal of both nuclides to the sea floor. Kd does not, however, have any direct bearing on the depth of last equilibration which is controlled by particle cycling and settling rates. The average depth of scavenging in the model is therefore general to all nuclides undergoing reversible scavenging, regardless of their Kd.

The model input is a 5500 m water-column profile of a nuclide concentration which would be expected from a 1D reversible scavenging model [38] at equilibrium. For Th, this would equate to a linear increase in ^{230}Th concentration with depth from zero at the surface to 2 dpm/1000 l at 5500 m. Large particles settle through the model water column (at rate, S, in m/day). As they fall, a fraction dissolves in each box, returning nuclides to the dissolved phase, and the remainder is allowed to disaggregate at the prescribed rate (r_{-1}). For particles settling from one box, therefore, some disaggregate in the box immediately below, while others fall further into deeper boxes or to the sediment before disaggregating.

The median depth of last scavenging was found to be insensitive to the particle concentration, to the distribution coefficient, and to the aggregation rate. Only processes that directly control the transport of large particles to the seafloor affect the depth of last scavenging. The affect of varying the settling rate, S, which drives transport to the seafloor, and disaggregation rate, r_{-1}, which inhibits transport to the seafloor, are shown in Fig. 7. Varying dissolution, γ, will have a similar effect to that of disaggregation because it prevents scavenged nuclides from sinking by returning them to the dissolved phase. A typical profile of the cumulative proportion of nuclide last scavenged at depth z is shown in Fig. 8. Varying S and r_{-1} within reasonable limits (S is typically $\approx$ 100 m day^{-1} [39] and r_{-1} varies from 150–750 yr^{-1} [40]) indicates that the median depth of final scavenging is unlikely to be more than 700 m from the seabed. Shallow median final scavenging can only be achieved in the model if disaggregation is unrealistically slow ($<$50 yr^{-1}) or the settling rate of large particles unrealistically fast ($>$600 m day^{-1}). Of course, if large particles effectively disaggregate on the seafloor and are able to exchange with seawater there, then the depth of median final scavenging is even deeper. The model therefore represents a maximum distance from the seabed from which dissolved Th and Pa are scavenged. Sedimentary Pa/Th ratios are therefore reflective of conditions in the bottom-most waters.

Because it is the processes of particle settling and disaggregation that control the depth of final scaveng-

Table 2
Abbreviations, units and values used in the 1D model

Variable	Abbreviation	Units	Values used	Reference
Nuclide concentration	N	dpm/1000 l^{-1}	Linear increase from 0 at surface to 2.01 at 5500 m	[51]
Particle concentration	P_s+P_l	g m^{-3}	Particle model giving 0.015 to 0.011 below 1500 m	[37]
Partition coefficient	Kd		10^6	
Aggregation	r_1	yr^{-1}	4	[37]
Disaggregation	r_{-1}	yr^{-1}	150	[37,40]
Dissolution	γ	yr^{-1}	0.025–50	[37]
Settling rate	S	m day^{-1}	150–600	[39]

References provide the source of these values.

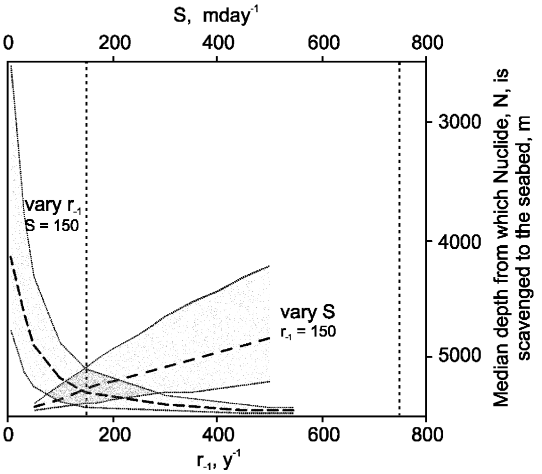

Fig. 7. Model sensitivity tests varying the settling rate, S, and the disaggregation rate, r_{-1}. The dashed lines indicate a sensible range for r_{-1} in deep waters as determined by Nozaki et al. [40]. The shaded areas indicate the inter-quartile range for the depth of scavenging. Note that, for all reasonable values of S and r_{-1}, most of nuclide, N, is scavenged within 700 m of the seafloor.

ing of nuclides, the results hold for both ^{230}Th and ^{231}Pa. Although large particles will have a relatively lower concentration of ^{231}Pa than ^{230}Th, leading to slower removal of ^{231}Pa, the depth in the water column from which it is last scavenged will be the same as for ^{230}Th. Thus, the ^{231}Pa/ ^{230}Th records in sediment cores can be used to investigate changes in the past chemistry and flow rate of near-bottom water masses. The chemistry of these water masses may, in turn, be influenced by water masses which overlie them, but this influence may take long enough to exert itself that waters will have travelled a significant distance. At sites where water masses have distinct ^{231}Pa concentrations, due to differing scavenging and advection histories, it is the lowermost water mass that will dominate the ^{231}Pa/^{230}Th signal recorded in the sediment. In the Indian Ocean, and in particular the Madagascar and Mascarene Basins, sedimentary ^{231}Pa/^{230}Th will therefore reflect the advection and scavenging history of Antarctic Bottom Water filling the basins.

5.3. *Implications for interpretation of sedimentary ^{231}Pa/^{230}Th records in other regions*

The realisation that sedimentary Pa/Th values reflect only the deepest water mass has implications for previous studies of sedimentary ^{231}Pa/^{230}Th in the North Atlantic [10,13]. In the modern ocean, NADW represents the deepest water mass in the North Atlantic so that core-top sedimentary ^{231}Pa/^{230}Th is likely to reflect the ventilation and productivity of this water mass. This situation was not necessarily always the case, however. If NADW were to shoal so that the deepest water mass was from a Southern-Ocean source, this Southern-Ocean source would control sedimentary ^{231}Pa/^{230}Th. Due to the long transport distance, and hence, long time during which to reach equilibrium, such Southern Ocean water masses would have high ^{231}Pa/^{230}Th, leading to values exported to the underlying sediment close to the production ratio. Such production ratio values have, for Heinrich 1 (H1) and the Younger Dryas, been proposed to represent periods of MOC shutdown or partial shut down [10]. This proposal is based on the assumption that sedimentary ^{231}Pa/^{230}Th is controlled by the whole water column. The modelling presented here, however, suggests that the MOC may have persisted during these intervals, but at a shallow depth. It should be stressed that this results does not preclude complete cessation of MOC at H1 as previously suggested. It just indicates that the ^{231}Pa/^{230}Th data may have another explanation.

The fact that sedimentary Pa/Th reflects only the deepest water mass may make it more difficult to provide an unambiguous interpretation of a single sedimentary record of Pa/Th. Such records might be interpreted, however, by the additional use of other proxies, particularly by the information provided by a water-mass tracer such as Cd/Ca or Nd isotopes. On the other hand, the fact that sedimentary Pa/Th allows recon-

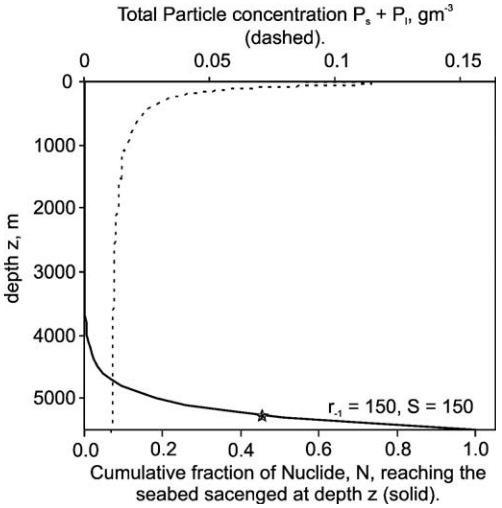

Fig. 8. Model results for the most realistic case, where settling rate, $S=150$ m day^{-1} and disaggregation rate, $r_{-1}=150$ yr^{-1}. Solid line shows the cumulative fraction of total nuclide, N, reaching the seafloor scavenged above a particular depth. The dashed line indicates the particle concentration profile used for this model (after [37]). The star is the median depth of scavenging (200 m above the seafloor).

struction of a particular water mass is good news for its application to multiple cores. A set of Pa/Th records from varying water masses should allow the history of flow rate to be reconstructed for all water masses at that location, rather than averaging flow over the whole water column.

The findings of this study also have implications for the use of sedimentary ^{231}Pa/^{230}Th as tools to investigate particle flux [41] and particle type [19]. Because the ^{231}Pa/^{230}Th exported to the sediments is most representative of the bottommost water mass, it is the particle flux and type at this depth, rather than at the surface, that will be reflected in the sedimentary ^{231}Pa/^{230}Th ratio.

6. Conclusions

The first ^{230}Th and ^{231}Pa water column profiles have been presented for the south western Indian Ocean. The ^{230}Th profile is similar to the average of previous measurements around the world's oceans. The ^{231}Pa profiles indicate that waters flowing from the Southern Ocean (AAIW, AABW) have experienced ^{231}Pa loss, probably due to removal by scavenging during transit through the opal belt. The high ^{231}Pa of NADW is preserved as a water mass tracer into the Indian Ocean, probably because this water mass does not enter the opal belt. The observation of water masses with distinct ^{231}Pa values in a single water column raises the question of which water mass controls the sedimentary Pa/Th values. A simple 1D model demonstrates that this sedimentary ^{231}Pa/^{230}Th signal is derived from the bottom ~1000 m of the water column, rather than averaging the whole water column. In the region of the Indian Ocean investigated here, this indicates that sedimentary records can be used to reconstruct the past flow rate of AABW into the Indian Ocean. The importance of bottom water for sedimentary Pa/Th records should also be considered when interpreting sedimentary ^{231}Pa/^{230}Th ratios from other regions.

Acknowledgements

We thank Nick McCave, the crew and scientific party aboard the R.R.S. *Charles Darwin* (cruise CD 129), for providing a platform for and helping with sample collection. We would also like to thank Dr Nick Belshaw for his help with the mass spectrometry, and two anonymous reviewers for their constructive comments. This work was supported with a Natural Environmental Research Council studentship No:NER/S/A/2002/10531.

References

[1] W.S. Broecker, The great ocean conveyor, Oceanography 4 (1991) 79–89.

[2] J.-C. Duplessy, N.J. Shackleton, R.K. Matthews, W. Prell, W.F. Ruddiman, M. Caralp, C.H. Hendy, ^{13}C Record of benthic foraminifera in the last interglacial ocean: implications for the carbon cycle and the global deep water circulation, Quaternary Research 21 (1984) 225–243.

[3] E.A. Boyle, Paired Cd and δ^{13}C data from benthic foraminifera: implications for ocean circulation, phosphorus, and atmospheric CO_2, Geochimica et Cosmochimica Acta 50 (1986) 265–276.

[4] R.L. Rutberg, S.R. Hemming, S.L. Goldstein, Evidence for decreased NADW flux during glacial stages 2 and 4 from Nd isotopes in Southern Ocean sediments, Mineralogical Magazine 62 (1998) 1304–1305.

[5] J.F. Adkins, H. Cheng, E.A. Boyle, E.R.M. Druffel, R.L. Edwards, Deep-sea coral evidence for rapid change in ventilation of the deep North Atlantic 14,400 years ago, Science 280 (1998) 725–728.

[6] S.J. Goldstein, D.W. Lea, S. Chakraborty, M. Kashgarian, M.T. Murrell, Uranium-series and radiocarbon geochronology of deep-sea corals; implications for Southern Ocean ventilation rates and the oceanic carbon cycle, Earth and Planetary Science Letters 193 (2001) 167–182.

[7] G.G. Bianchi, I.R. Hall, I.N. McCave, L. Joseph, Measurement of the sortable silt current speed proxy using the Sedigraph 5100 and Coulter Multisizer IIe: precision and accuracy, Sedimentology 46 (1999) 1001–1014.

[8] I.N. McCave, B.E. Tucholke, Deep current-controlled sedimentation in the western North Atlantic, in: P.R. Vogt, B.E. Tucholke (Eds.), The Geology of North America M, The Western North Atlantic Region, Geological Society of America, Am., 1986.

[9] O. Marchal, R. Francois, T.F. Stocker, F. Joos, Ocean thermohaline circulation and sedimentary ^{231}Pa/^{230}Th ratio, Paleoceanography 15 (2000) 625–641.

[10] J.F. McManus, R. Francois, J.-M. Gherardi, L. Keigwin, S. Brown-Leger, Collapse and rapid resumption of Atlantic meridional circulation linked to deglacial climate changes, Nature 428 (2004) 834–837.

[11] J.F. McManus, R. Francois, J.M. Gherardi, J. Nuwer, Variable rates of ocean circulation from sedimentary ^{231}Pa/^{230}Th during the last ice age, Goldchmidt Conference Abstracts, 2002, pp. A503.

[12] J.C. Scholten, M.M. Rutgers van der Loeff, A. Michel, Distribution of ^{230}Th and ^{231}Pa in the water column in relation to the ventilation of the deep Arctic basins, Deep-Sea Research Part II: Topical Studies in Oceanography 42 (1995) 1519–1531.

[13] E.F. Yu, R. Francois, M.P. Bacon, Similar rates of modern and last-glacial ocean thermohaline circulation inferred from radiochemical data, Nature 379 (1996) 689–694.

[14] J.H. Chen, R.L. Edwards, G.J. Wasserburg, ^{238}U, ^{234}U and ^{232}Th in seawater, Earth and Planetary Science Letters 80 (1986).

[15] T.L. Ku, K.G. Knauss, G.G. Matthieu, Uranium in the open ocean: concentration and isotopic composition, Deep Sea Res 11 (1977) 1005–1018.

[16] G.M. Henderson, Seawater (^{234}U/^{238}U) during the last 800 thousand years, Earth and Planetary Science Letters 199 (2002) 97–110.

[17] M.P. Bacon, R.F. Anderson, Distribution of thorium isotopes between dissolved and particulate forms in the deep sea, Journal of Geophysical Research 87 (1982) 2045–2056.

[18] G.M. Henderson, R.F. Anderson, The U-series toolbox for paleoceanography, Reviews in Mineralogy and Geochemistry “Uranium Series Geochemistry” 53 (2003) 493–531 (MSA).

[19] Z. Chase, R.F. Anderson, M.Q. Fleisher, P.W. Kubik, The influence of particle composition and particle flux on scavenging of Th, Pa and Be in the ocean, Earth and Planetary Science Letters 204 (2002) 215–219.

[20] W. Geibert, R. Usbeck, Adsorption of thorium and protactinium onto different particle types: Experimental findings, Geochimica et Cosmochimica Acta 68 (2004) 1489–1501.

[21] S. Luo, T.-L. Ku, Oceanic ^{231}Pa/^{230}Th ratio influenced by particle composition and remineralization, Earth and Planetary Science Letters 167 (1999) 183–195.

[22] M. Siddall, T.F. Stocker, G. Henderson, M.N.R. Edwards, S.A. Muller, F. Joos, M. Frank, ^{231}Pa/^{230}Th fractionation by ocean transport, biogenic particle flux and particle type, Earth and Planetary Science Letters 237 (2005) 135–155.

[23] Y.-H. Li, Controversy over the relationship between major components pf sediment-trap materials and the bulk distribution coefficents of ^{230}Th, ^{231}Pa, and ^{10}Be, Earth and Planetary Science Letters 233 (2005) 1–7.

[24] M.M. Rutgers van der Loeff, G.W. Berger, Scavenging of ^{230}Th and ^{231} Pa near the Antarctic Polar Front in the South Atlantic, Deep-Sea Research Part I: Oceanographic Research Papers 40 (1993) 339–357.

[25] J.M. Toole, B.A. Warren, A Hydrographic Section across the Subtropical South Indian Ocean, Deep-Sea Research Part I—Oceanographic Research Papers 40 (1993) 1973–2019.

[26] K.A. Donohue, J.M. Toole, A near-synoptic survey of the Southwest Indian Ocean, Deep-Sea Research Part II: Topical Studies in Oceanography 50 (2003) 1893–1931.

[27] A. Sirinvasan, Z. Top, P. Schlosser, R. Hohmann, M. Iskandarani, D.B. Olson, J.E. Lupton, W.J. Jenkins, Mantle ^{3}He distribution and deep circulation in the Indian Ocean, Journal of Geophysical Research, C, Oceans 109 (2004) C06012.

[28] M. Tomczak, J.S. Godfrey, Regional oceanography: An introduction, 2002.

[29] I.N. McCave, T. Kiefer, D.J.R. Thornalley, H. Elderfield, Deep flow in the Madagascar–Mascarene Basin over the last 150,000 years, Proceedings of the Royal Society, vol. 363, 2004, pp. 1–19.

[30] L.F. Robinson, N.S. Belshaw, G.M. Henderson, U and Th concentrations and isotope ratios in modern carbonates and waters from the Bahamas, Geochimica et Cosmochimica Acta 68 (2004) 1777–1789.

[31] K. Usman, T.D. MacMahon, Determination of the half-life of ^{233} Pa, Applied Radiation and Isotopes 52 (2000) 585–589.

[32] M. Regelous, S.P. Turner, T.R. Elliott, K. Rostami, C.J. Hawkesworth, Measurement of femtogram quantities of protactinium in silicate rock samples by multicollector inductively coupled plasma mass spectrometry, Analytical Chemistry 76 (2004) 3584–3589.

[33] M.S. Choi, R. Francois, K. Sims, M.P. Bacon, S. Brown-Leger, A.P. Fleer, L. Ball, D. Schneider, S. Pichat, Rapid determination of ^{230}Th and ^{231}Pa in seawater by desolvated micro-nebulization Inductively Coupled magnetic sector mass spectrometry, Marine Chemistry 76 (2001) 99–112.

[34] H.U. Sverdrup, M.W. Johnson, R.H. Fleming, The oceans, their physics, chemistry, and general biology, Prentice and Hall, New York, 1942, 1087 pp.

[35] H.J. Walter, M.M. Rutgers van de Loeff, H. Hoeltzen, Enhanced scavenging of ^{231}Pa relative to ^{230}Th in the South Atlantic south of the Polar Front: Implications for the use of the ^{231}Pa/^{230}Th as a paleoproductivity proxy, Earth and Planetary Science Letters 149 (1997) 85–100.

[36] L. Dezileau, G. Bareille, J.L. Reyss, The ^{231}Pa/^{230}Th ratio as a proxy for past changes in opal fluxes in the Indian sector of the Southern Ocean, Marine Chemistry 81 (2003) 105–135.

[37] S.L. Clegg, M. Whitfield, A generalized model for scavenging of trace metals in the open ocean—II. Thorium scavenging, Deep Sea Research 38 (1991) 91–120.

[38] S.B. Moran, C.-C. Shen, S.E. Weinstein, L.H. Hettinger, J.H. Hoff, H.N. Edmonds, R.L. Edwards, Constraints on the deep water age and particle flux in the Equatorial and South Atlantic Ocean based on seawater ^{231}Pa and ^{230}Th data, Geophysical Research Letters 28 (2001) 2440–3437.

[39] M.P. Bacon, C.-A. Huh, A.P. Fleer, W.G. Deuser, Seasonality in the flux of natural radionuclides and plutonium in the deep Sargasso Sea, Deep Sea Research 32 (1985) 273–286.

[40] Y. Nozaki, H.-S. Yang, M. Yamada, Scavenging of thorium in the ocean, Journal of Geophysical Research 92 (1987).

[41] N. Kumar, R. Gwiazda, R.F. Anderson, P.N. Froelich, ^{231}Pa/^{230}Th ratios in sediments as a proxy for past changes in Southern Ocean productivity, Nature (London) 362 (1993) 45–48.

[42] J. Robert, C.F. Miranda, R. Muxart, Mesure de la periode du protactinium-231 par microcalorimetrie, Radiochimica Acta 11 (1969) 104–108.

[43] H. Cheng, R.L. Edwards, J. Hoff, C.D. Gallup, D.A. Richards, Y. Asmerom, The half lives of uranium-234 and thorium-230, Chemical Geology 169 (2000) 17–33.

[44] N.E. Holden, Total half-lives of selected nuclides, Pure and Applied Chemistry 62 (1990) 941–958.

[45] T.-L. Ku, Uranium series disequilibrium in deep sea sediments, Ph.D, Columbia, 1966.

[46] O. Ragueneau, P. Trefuer, A. Leynaert, R.F. Anderson, M.A. Brzezinski, D.J. DeMaster, R.C. Dugdale, J. Dymond, G. Fisher, R. Francois, C. Heinze, E. Maier-Reimer, V. Martin-Jezequel, D.M. Nelson, B. Queguiner, A review of the Si cycle in the modern ocean: Recent progress and missing gaps in the application of biogenic opal as a paleoproductivity proxy, Global and Planetary Change 20 (2000) 317–365.

[47] T.P. Boyer, C. Stephens, J.I. Antonov, M.E. Conkright, R.A. Locarnini, T.D. O’Brien, H.E. Garcia, Salinity, in: S. Levitus (Ed.), World Ocean Atlas 2001, NOAA Atlas NESDIS, vol. 50 2, U.S. Government Printing Office, Wash., D.C, 2002, p. 165.

[48] M.E. Conkright, H.E. Garcia, T.D. O’Brien, R.A. Locarnini, T.P. Boyer, C. Stephens, J.I. Antonov, Nutrients, in: S. Levitus (Ed.), World Ocean Atlas 2001, NOAA Atlas NESDIS, vol. 52 4, U.S. Government Printing Office, Wash., D.C, 2002, p. 392.

[49] S.L. Clegg, M. Whitfield, A generalized model for the scavenging of trace metals in the open ocean—I. Particle cycling, Deep Sea Research 37 (1990) 809–832.

[50] C.-A. Huh, Th isotopes in the Santa Monica Basin: temporal variation, long-term mass balance and rate constants, Journal of Oceanography 15 (1995) 363–373.

[51] S.B. Moran, M.A. Charette, J.A. Hoff, R.L. Edwards, W.M. Landing, Distribution of ^{230}Th in the Labrador Sea and its relation to ventilation, Earth and Planetary Science Letters 150 (1997) 151–160.